Proceedings of the Korean Nuclear Society Autumn Meeting
Seoul, Korea, October 1998

Neutron Production from Spallation Reactions

Jaegwon Yoo
Korea Atomic Energy Research Institute
P.O. Box 105 Yusung, Taejon 305-600 Korea

Abstract

Target systems for spallation neutrons are designed to enhance production and neutronic efficiencies as well as to investigate a target cooling system. Lead and tungsten are chosen for target materials. Three target systems (solid cylinder, solid disc array, disc-array in cylindrical shell) for applications to a subcritical fast reactor are introduced to investigate neutronic characteristics of each target geometry. By making use of LCS simulation code, neutron production and leakage rates are calculated for each target design. The cost effective neutron yields turns out to be ~27 n/s at 1.3 GeV for solid lead target, and ~24 n/s at 1.5 GeV for solid tungsten target, per an incident proton. Single proton from 1 GeV accelerator deposits total heat of 588 MeV in solid lead target and 600 MeV in solid tungsten target. As far as spallation neutron yields and heat removal system design are concerned, lead target system has advantage of the tungsten target. By adjusting size of solid lead target, the optimal radius and height of the target are found to be ~11 cm, and ~50 cm, respectively. Energy spectra of neutron fluxes of the tungsten target system shows much better performance than those of lead target in the energy range of lower than 1 MeV. Relation of the size of target and axial distributions of neutron fluxes is discussed in this paper. Also, we present a method to reduce leakages through top and bottom surfaces by adjusting a gap distance of disc-array type target system. Our neutronic results obtained from lead target can also be applied to liquid lead target system except for heat removal mechanisms.

I. Introduction

Since neutron is an electrically neutral massive particle with a spin 1/2, neutron can play an important role in studying fundamental physics. Neutron beams are one of the most useful probes of solid condensed matter physics and material sciences such as solids, liquids, polymers, and biological systems. Because of the charge neutrality, neutrons interact only weakly with matter via short-range nuclear reaction so as to penetrate a few cm of solids with little attenuation. The spin magnetic moment of neutrons can interact very efficiently with the magnetic moment of solid. The traditional sources for neutron beams are research reactors where a continuous stream of neutrons is produced in the fission reaction. Recently, accelerator-based spallation sources, in which high-energy protons bombarded heavy nuclei and make loose neutrons, have become available. In general, neutron moderation is less complete in the spallation sources and, consequently, they have more high-energy neutrons than the reactor-based sources. Roughly speaking, 1 mA of proton beams from 1 GeV accelerator is capable of producing spallation neutron beams of 10^{17} n/s. Intense neutron fluxes from spallation sources can be used in a variety of applications such as accelerator-based subcritical reactor for energy production[1] and/or waste incineration[2], radioisotope production for medical applications as well as basic science research.

Spallation is a nuclear reactions that are caused by energetic (> 100 MeV) particles interacting with an atomic nucleus. Spallation target design requires to consider many aspects of physics and engineering problems such as maximization of total neutron production inside the target material, efficient neutron leakage, reduction of neutron leakage in unwanted directions, radiation damage resistance, and mechanical problems as well as target cooling problems. In this paper, we investigate neutronic characteristics of the various shapes of spallation targets composed of two typical heavy element materials, lead and tungsten, bombarded by proton beams from 1GeV accelerator, since the number of neutrons produced from spallation reaction depends on target material and size, and the energy of incident protons. Section II begins with a brief introduction to microscopic spallation mechanisms. We discuss basic designs of solid cylinder, disc-array type, and disc-array in cylindrical shell target systems to enhance macroscopic spallation cross sections. Also computational tools (LCS) for simulating spallation are briefly introduced. Presenting our discussions based on results of neutronics and heat depositions of each target and material in Section III, we made a conclusive summary in Section IV.

II. Spallation Targets

In spallation processes of high-energy protons with atomic nucleus, since the collision time between the incident proton and a nucleon is relatively shorter than the mean collision between nucleons inside the atomic nucleus, the collision process can be modeled by a collision between the incoming proton and a nucleon, where the atomic nucleus plays a role of a source of level density above the Fermi sea level. Spallation process can be splitted into two stages of reaction inside an atomic nucleus, the intranuclear cascade and the evaporation cascade. The intranuclear cascade leads to a series of direct reactions ejecting nucleons or fragmentation of nucleus from atomic nucleus. The nuclei are in excited states after the intranuclear cascade reactions and then they make transitions to their ground state by emitting evaporating nucleons. From evaporation cascade process, mostly neutrons are coming out because of Coulomb barrier.

Since spallation neutron yields depend on macroscopic cross-sections and target materials, target design requires consider various aspects of physics and engineering in detail. The target material should be neutron rich heavy element and radiation damage resistive. Depending on requirements of a specific application, there are many parameters to be considered in designing spallation target system. In many applications, a high neutron flux is most desirable. In the subcritical breeder reactor, even though the blanket is generally exposed to unmoderated neutrons from the target, large neutron yields may be more desirable than high flux of neutrons, since some moderation inevitably takes in the blanket itself. To enhance macroscopic spallation cross-sections, evaluations of performances should be carried out with different shapes and sizes of targets. Bearing external neutron sources for a subcritical fast reactor in mind, we evaluate neutronic performances with three basic target designs composed of lead and tungsten as shown in Figs. 1(solid cylinder), 2 (disc-array type) and 3 (disc-array surrounded by a cylindrical shell). Because this application requires high flux neutrons, spallation targets should be compact and capable of cooling high power densities. For other applications, thick slab type target and/or array of slabs can be considered, since a detail target design should be done to meet specific application requirements

LCS[3] is developed by linking two major modules of LAHET and HMCNP[4] via neutron file (NEUTP). Particle transport in both LAHET and MCNP is based on Monte-Carlo algorithm. LAHET calculates the production and transport of all particles, such as protons, pions, muons and neutrons, based on the Bertini tape, and on models of direct reactions, evaporations, and fissions. LAHET uses a pre-equilibrium model for intermediate stages between the intranuclear cascade and the evaporation phases. It requires neutron having energy higher than cutoff, 20 MeV, in calculating neutron interactions based on simple cross section models. To calculate source neutrons, we execute LAHET with inputs of incident proton energies and fluxes, flux profile and size, information of injection point and a nuclear list of target material, and geometry description of the target system. Outputs of LAHET are neutron yields, deposition power, neutron source with spatial and energy resolutions, Edited tallies of the initial LAHET execution are obtained by the subsequent processing of data recorded on the history file (HISTP) generated from the HTAPE code. The history file may contain a complete description of the events occurred during the computation with LAHET. Any neutron appearing from a reaction with energy below the cutoff energy has its kinematic parameters recorded on a neutron file (NEUTP) for using subsequent transport computation with HMCNP. Since the LCS is based on a coupling LAHET to HMCNP via the neutron file, HMCNP uses the same geometry as in LAHET. Neutron source of LAHET output is fed into the input of HMCNP. The outputs of HMCNP are neutron fluxes, thermal power, one-group cross section, and neutron spectra.

III. Results and Discussions

Neutron yields are calculated with solid lead (Pb) and tungsten (W) targets bombarded by a high-energy proton, since the number of neutrons produced from spallation reaction depends on target material and size, and the energy of incoming proton. For every single proton production in spallation reactions, the cascade process yields about two neutrons, on the other hand, the evaporation process emits about 10 neutrons. The majority (80%) of neutrons turns out to be produced from evaporation process, while spallation protons are emitted almost equally from the cascade and the evaporation processes.

Figures 4 and 5 show that neutron productions are almost linearly proportional to the incident proton energy in the range of 1~5 GeV. Because of larger atomic density of tungsten than that of lead, the ratio of neutron productions for each material is nearly proportional to the cubical root of the ratio of atomic densities. Most neutrons produced inside the target, eventually, can leak through surfaces (top, bottom, cylinder) of the lead target (leakage rate=99%); for the tungsten target, however, the total leakage of neutrons is significantly less than neutron production (leakage rate=71%), since the absorption cross section of tungsten is much larger than that of

lead. Furthermore the leakage through cylindrical surface of tungsten target (72%) is smaller than that of lead target (78%); mostly due to the leakage through top surface (24%) of tungsten target (compare with 14% of top leakage for lead target). The greater bottom leakage (8%) for lead target (compare with 4% of bottom leakage for tungsten target) also supports smaller absorption cross section of lead. Note that the production, leakage plots in Fig. 4 and 5 show small deviations from straight line. If these small curvatures are magnified by incoming proton energy of 1 GeV equivalance, the most efficient proton energies for making cost effective spallation neutron yields can be determined as shown in Figs. 4 and 5; solid lead target can release ~27 n/s at 1.3 GeV, for tungsten target, ~24 n/s are emitted at 1.5 GeV. Comparing neutron leakage performance of two target materials, lead target. As far as spallation neutron yields are concerned, lead target system has advantage of tungsten target system.

Even though the total heat deposition of the solid tungsten target, 600 MeV, is only 2% larger than that of the solid lead target, 587.8 MeV, per incident 1 GeV proton, the local patterns of heat depositions are quite different from material to material because of their bulk densities. The amount of energy deposited per neutron produced inside the target material is plotted in Figs 6 (solid lead target) and 7 (solid tungsten target). In general, the heat builds up largely inside the bombardment area of proton beams on the top of the targets, and it is getting smaller and smaller as the depth distance increases. Heat deposition drops very quickly outside of the beam bombardment area. The local maximum heat deposition rate of solid tungsten target is 65% larger than that of solid lead target. One of the best ways to disperse the local heat deposition is to increase the proton beam radius, in which the local peak decreases inversely proportional to the beam cross section. In a viewpoint of heat removal system design, the solid lead target is preferable to the solid tungsten target.

Due to the neutron scattering and absorption processes inside the target, spallation neutron leakages through each surface depend on the size of target system. For an 1 GeV proton beam bombarding a solid lead target, neutron yields versus radii of target at a fixed height of 50 cm is plotted in Fig. 8, and Fig. 9 is a plot of neutron yields versus heights of target at a fixed radius of 15 cm. Figure 8 shows that the neutron yields rapidly increase up to 11 cm of radius mostly through cylinder surface, and that the increase of them between 11~40 cm is mostly due to the neutrons ejected through top and bottom surfaces, whereas the cylinder surface contribution keeps decreasing. Beyond this radius the total neutron yield is getting saturated. Figure 9 shows that the neutron yields versus the height of cylinder. Up to 12 cm of height, most neutrons are coming out through top and bottom surfaces, whereas most neutrons are emitted through cylinder surface for longer than 60 cm of height. Characteristically unique feature of height dependence is that the bottom leakage has its peak at ~16 cm and the top leakage is getting saturated beyond ~20 cm. In most cases of applications, since it is desirable to have as many neutrons through cylinder surface as possible, a target shape should be properly designed to reduce the top leakage, which also can cause radiation damages on the surface of beam window system.

On average, energy spectra of neutron fluxes are plotted in Figs. 10 and 11, respectively, for solid lead and tungsten targets. Notice that a direct comparison of neutron spectra in Figs. 10 and 11 are meaningful only in adjacent energy interval, since neutron spectra in those figures are scaled with lethargy. In low-energy range (< 0.2 MeV), the solid tungsten target performs much better than lead target, on the other hand, in high-energy range (> 1 MeV), the situation is reversed, thus it can be said that neutron moderation power of tungsten is much better than that of lead. The larger moderation power can be attributed to large top leakage of tungsten target shown in Fig. 5, since low-energy neutrons are relatively isotropic; conversely, comparably large bottom leakage of lead target can be attributed to smaller moderation power of lead shown in Fig.6, since high-energy neutrons are extremely penetrating.

Spallation neutron yields from disc-array type target of Fig. 2 are plotted in Figs. 12 (for lead) and 13 (for tungsten). For lead target system, neutron production rate decreases, as the gap width increases, due to larger leakage rate of neutrons through cylinder surface that makes fewer collisions inside the target. So the total leakage decreases due to less neutron production. The bottom leakage decreases more rapidly than the top leakage as gap width increases from zero to ~3 cm because of bouncing back of high-energy neutrons between discs. Top leakage also decreases from zero to ~20 cm of gap width, and then it saturates for greater than 20 cm of gap width. For small gap distances, isotropic low-energy neutrons leaking through cylinder surface increases as the surface area increases. For large gap distances, on the other hand, high-energy neutrons bouncing back from first few discs, where the flux is almost constant due to relatively well collimated neutron streams, are responsible for constant top leakage. Similar arguments made in lead target system can be applicable to a tungsten disc-array target except for a few subtleties occurring in small gap width. For a tungsten target, contrast to a lead target, the top leakage decreases more rapidly than the bottom leakage in first ~3 cm due to the

moderation power of tungsten. The moderation power of tungsten explains a quick increase of the neutron leakage through cylinder surface and a local peak of total leakage occurred at gap width of ~1.5 cm.

Spallation neutron yields from disc-array surrounded by a cylindrical shell type target of Fig. 3 are plotted in Figs. 14 (for lead) and 15 (for tungsten disc-array surrounded by a lead shell). Basically neutron production and leakage mechanism are very similar to the case of disc-array type targets. For lead target system, neutron production rate increases at large gap width, since neutrons, for larger gap widths, are less collimated to enter and make collisions inside the cylindrical shell. The neutron leakage increases in conjunction with neutron production. Cylindrical shell makes less decrease of the bottom and top leakages than the case of disc-array type target. Similar arguments made in lead target system can be applicable to a tungsten disc-array in lead shell target system. In a case of pure tungsten disc-array in cylindrical shell, the total leakage turns out to be considerably less than the total neutron production because of larger absorption cross section of tungsten. For a case of the tungsten disc-array in lead shell, the neutron production mechanism in disc-array zone is almost the same as disc-array target system. Neutron moderation power of tungsten discs yields relatively low-energy neutrons, and relatively isotropic neutrons. Since these neutrons make collisions in lead shell zone, the total production and leakage are nearly constant for large gap width.

Information of axial distributions of neutron spectra is as much important as radial neutron spectra in many applications. Neutron fluxes from cylinder surface of various target shapes are plotted in Figs 16 (for lead target) and 17 (for tungsten). For solid cylinder target systems, the peaks of flux distributions are occurred at around a first quarter of height from the top, where most neutron produced are moderated to be isotropic enough. Above this height, the solid tungsten target has less fluxes than the solid lead target due to more neutrons emitted through top surface, and larger moderation power of tungsten target. Furthermore, Below this height, the fluxes from the solid tungsten target is smaller than those from the solid lead target, since the neutrons are further moderated and absorbed. The plot for the tungsten disc-array target shows that bouncing process in gaps can explain valleys in discs and the crests in gaps. The bouncing effects in lead disc-array target are comparatively small, since the valley to crest is narrower than tungsten case as shown in Figs. 16 and 17. Notice that, for both materials, the axial positions of the peak are shifted downward due to the larger ratio of radius to height than solid cylinder targets. If a cylindrical shell surrounds disc-array type targets, the axial positions of the peak shift further downward because of increased ratio of radius to height.

IV. Summary

As mentioned above, target performance must be evaluated on the bases of application requirements. In this section we summarize evaluations of target performances for driving a subcritical fast reactor. In general, the spallation neutron yields are proportional to the energy of incident protons and the beam currents.

First of all, the target material should be neutron rich heavy element and radiation damage resistive as well as mechanically robust at high temperature. Tungsten and solid/liquid lead satisfy these requirements. To ease power densities in target system, primarily a proper cooling system need to be devised. In this case, coolant must have very small neutron absorption cross-section and small moderation power in cases of coupling with a fast reactor blanket. Since fast reactors require high neutron flux, liquid metal target/coolant system should be considered. Enlarging the radius of proton beam using defocusing magnetic lenses can relieve local power density buildups, which are inversely proportional to cross-sectional area of incident beam at the entrance point of targets.

Geometrical shape of targets should be simple and compact. Since the target shape determines the radial and axial distribution of neutron fluxes, axially symmetric target is designed in cylinder types such as a solid cylinder, a disc-array, and a disc-array surrounded by a cylindrical shell. Varying the size of target, we can optimize neutron leakage from each surface. For examples, the optimal radius of solid lead target for a fixed height of 50 cm turns out to be about 11 cm, and the optimal height of solid lead target for a fixed radius of 15 cm is about 50 cm. Adjusting disc-array target can reduce the top and bottom leakage. Especially this idea can be used to reduce the neutron streams toward the proton window. Furthermore, the ratio of radius to height controls axial distributions of neutron spectra, the larger the ratio, the more symmetric the axial distribution. However, it is not practically feasible to have such a large enough ratio of radius to height, which can be possible only for two extreme cases such as a single disc type or a long fat cylinder type. Therefore, the most optimal target design parameters for subcritical fast reactors can only be found by evaluating target performances for various target shapes and compositions beyond above basic designs.

References

[1] F. Carminati, C. Geles, R. Klapisch, J. P. Revol, CH. Roche, J. A. Rubio and C. Rubbia, "An Energy Amplifier for Cleaner and Inexhaustible Nuclear Energy Production Driven by a Particle Beam Accelerator," CERN/AT/93-47 (ET) (1993)

[2] Accelerator-Driven Systems: Energy Generation and Transmutation of Nuclear Waste. Status Report, IAEA, Vienna (1997)

[3] R. E. Prael, H. Lichtenstein, "User Guide to LCS: The LAHET Code System," LA-UR-89-3014, Los Alamos National Laboratory (1989)

[4] J. F. Briesmeister, "MCNP – A General Monte Carlo N-Particle Transport Code Version 4A," LA-12625-M (1993)

Figure 1. Solid cylinder target.

Figure 2. Disc-array type target.

Figure 3. Disc-array surrounded by a cylindrical shell.

Figure 4. Rate of neutron production and leakage for solid lead target. R=15 cm, H=50 cm, R_b=5 cm, E_b=1 GeV.

Figure 5. Rate of neutron production and leakage for solid tungsten target. R=15 cm, H=50 cm, R_b=5 cm, E_b=1 GeV.

Figure 6. Heat deposition in solid lead target. R=15 cm, H=50 cm, R_b=5 cm, E_b=1 GeV.

Figure 7. Heat deposition in solid tungsten target. R=15 cm, H=50 cm, R_b=5 cm, E_b=1 GeV.

Figure 8. Neutron yields of solid lead target at H=50 cm, R_b=5 cm, E_b=1 GeV.

Figure 9. Neutron yields of solid lead target at R=15 cm, H=50 cm, R_b=5 cm, E_b=1 GeV.

Figure 10. Neutron spectra of solid lead target. R=15 cm, H=50 cm, R_b=5 cm, E_b=1 GeV.

Figure 11. Neutron spectra of solid tungsten target. R=15 cm, H=50 cm, R_b=5 cm, E_b=1 GeV.

Figure 12. Lead disc-array target system.
R=15 cm, R_b=5 cm, E_b=1 GeV,
13 discs (thickness=2 cm), 12 gaps (width=2 cm).

Figure 13. Tungsten disc-array target system.
R=15 cm, R_b=5 cm, E_b=1 GeV,
13 discs (thickness=2 cm), 12 gaps (width=2 cm).

Figure 14. Lead disc-array in a cylinder shell.
R=15 cm, R_s=10 cm, R_b=5 cm, E_b=1 GeV,
13 discs (thickness=2 cm), 12 gaps (width=2 cm).

Figure 15. Tungsten disc-array in a cylinder shell.
R=15 cm, R_s=10 cm, R_b=5 cm, E_b=1 GeV,
13 discs (thickness=2 cm), 12 gaps (width=2 cm).

Figure 16. Axial distributions of neutron fluxes for lead targets. R=15 cm, H=10 cm, R_s=10 cm, R_b=5 cm, E_b=1 GeV, 13 discs (thickness=2 cm), 12 gaps (width=2 cm).

Figure 17. Axial distributions of neutron fluxes for tungsten targets. R=15 cm, H=10 cm, R_s=10 cm, R_b=5 cm, E_b=1 GeV, 13 discs (thickness=2 cm), 12 gaps (width=2 cm).

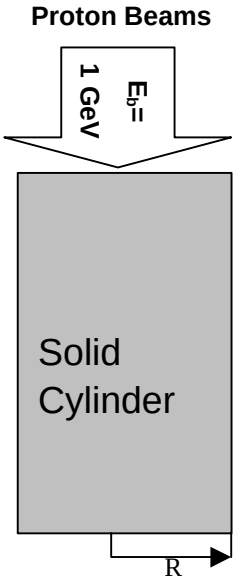

Figure 1. Solid cylinder target.

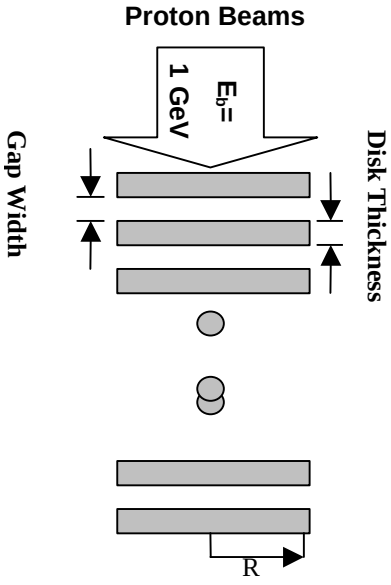

Figure 2. Disc-array type target.

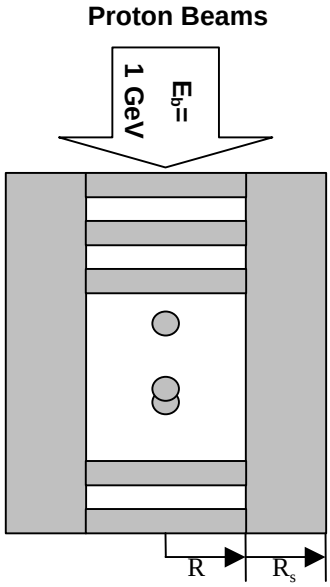

Figure 3. Disc-array surrounded by a cylindrical shell.

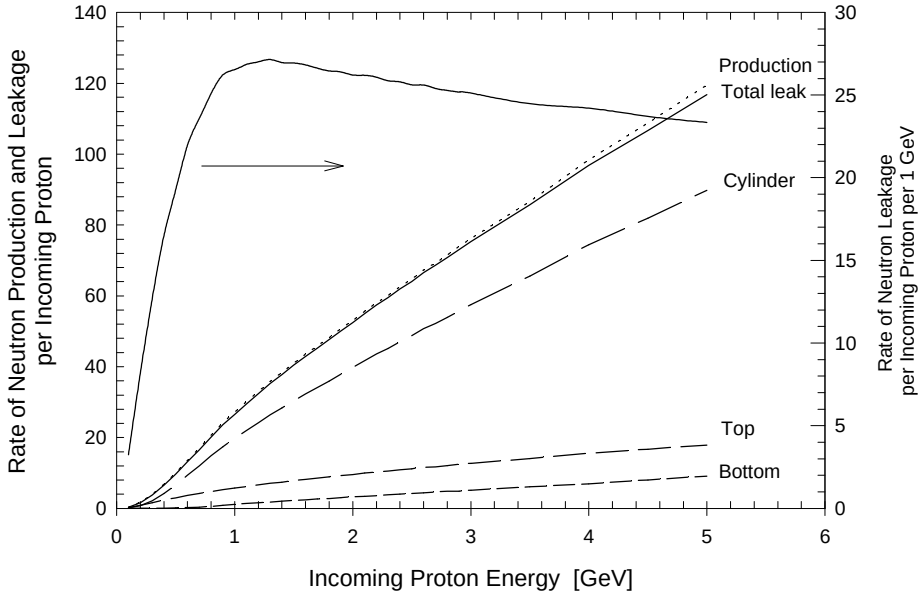
Rate of Neutron Production and Leakage per Incoming Proton
Rate of Neutron Leakage per Incoming Proton per 1 GeV
Incoming Proton Energy [GeV]
Production
Total leak
Cylinder
Top
Bottom
0
20
40
60
80
100
120
140
0
5
10
15
20
25
30
0
1
2
3
4
5
6

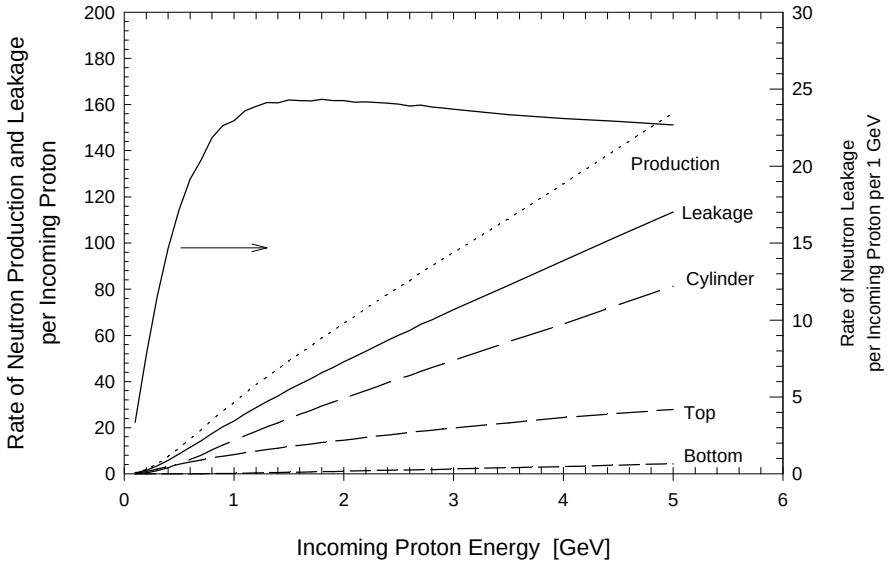
Rate of Neutron Production and Leakage
per Incoming Proton
Rate of Neutron Leakage
per Incoming Proton per 1 GeV
Incoming Proton Energy [GeV]
Production
Leakage
Cylinder
Top
Bottom
0
20
40
60
80
100
120
140
160
180
200
0
5
10
15
20
25
30
0
1
2
3
4
5
6

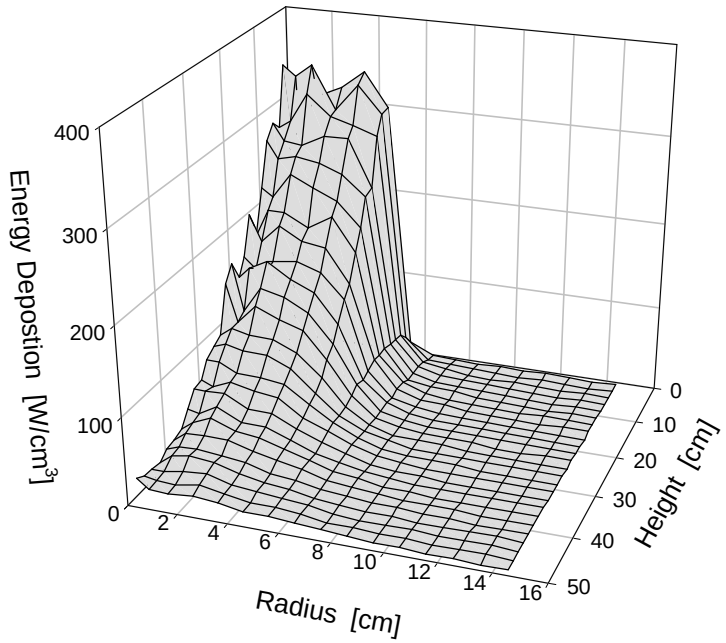
Energy Deposition [W/cm3]
400
300
200
100
0
0
2
4
6
8
10
12
14
16
Radius [cm]
0
10
20
30
40
50
Height [cm]

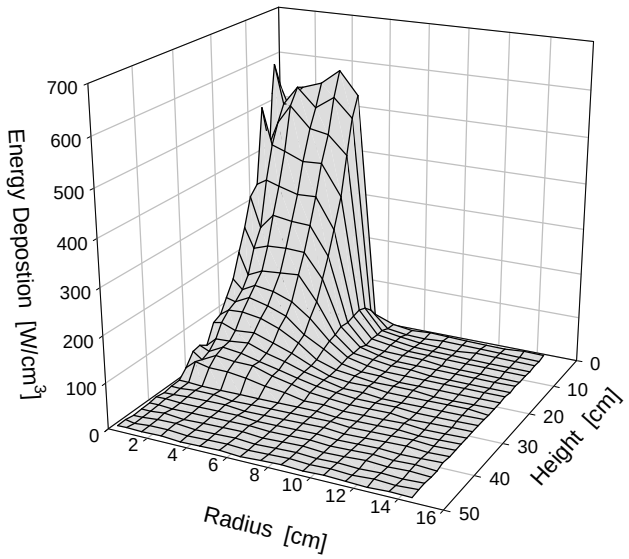
Energy Deposition [W/cm3]
700
600
500
400
300
200
100
0
2
4
6
8
10
12
14
16
Radius [cm]
0
10
20
30
40
50
Height [cm]

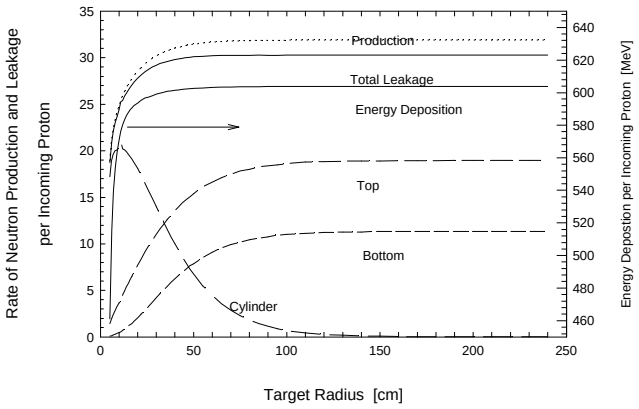
Rate of Neutron Production and Leakage
per Incoming Proton
Energy Deposition per Incoming Proton [MeV]
Target Radius [cm]
Production
Total Leakage
Energy Deposition
Top
Bottom
Cylinder
0
5
10
15
20
25
30
35
460
480
500
520
540
560
580
600
620
640
0
50
100
150
200
250

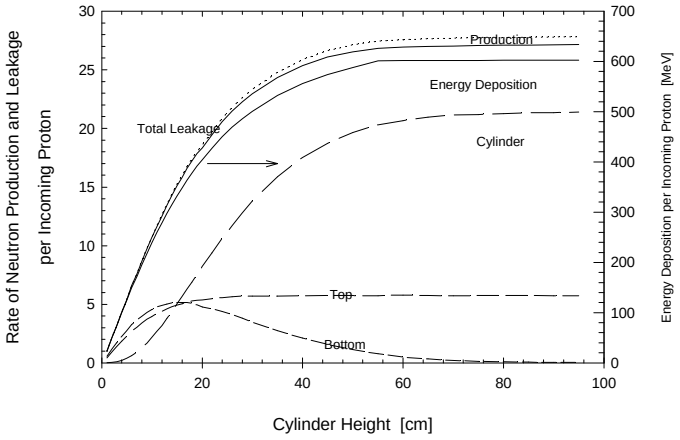
Rate of Neutron Production and Leakage
per Incoming Proton
Energy Deposition per Incoming Proton [MeV]
Cylinder Height [cm]
Production
Energy Deposition
Total Leakage
Cylinder
Top
Bottom
0
5
10
15
20
25
30
0
100
200
300
400
500
600
700
0
20
40
60
80
100

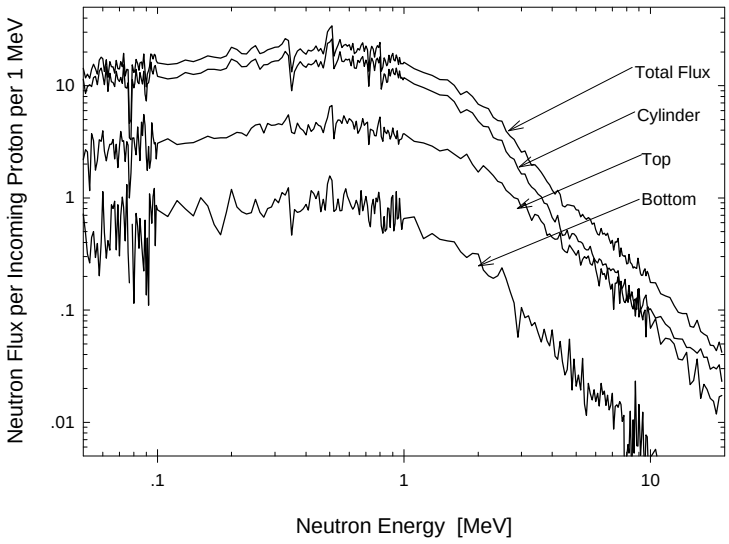
Neutron Flux per Incoming Proton per 1 MeV
10
1
.1
.01
.1
1
10
Neutron Energy [MeV]
Total Flux
Cylinder
Top
Bottom

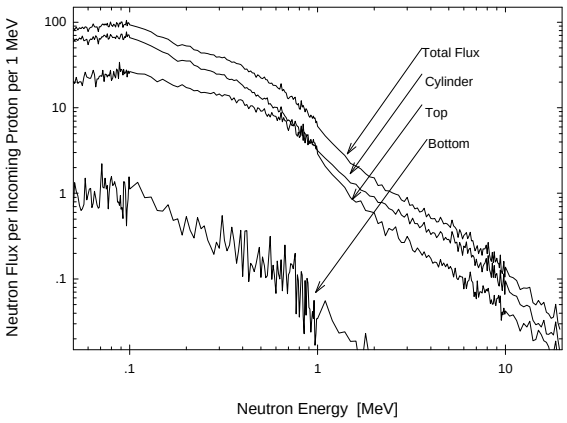
Neutron Flux per Incoming Proton per 1 MeV
100
10
1
.1
.1
1
10
Neutron Energy [MeV]
Total Flux
Cylinder
Top
Bottom

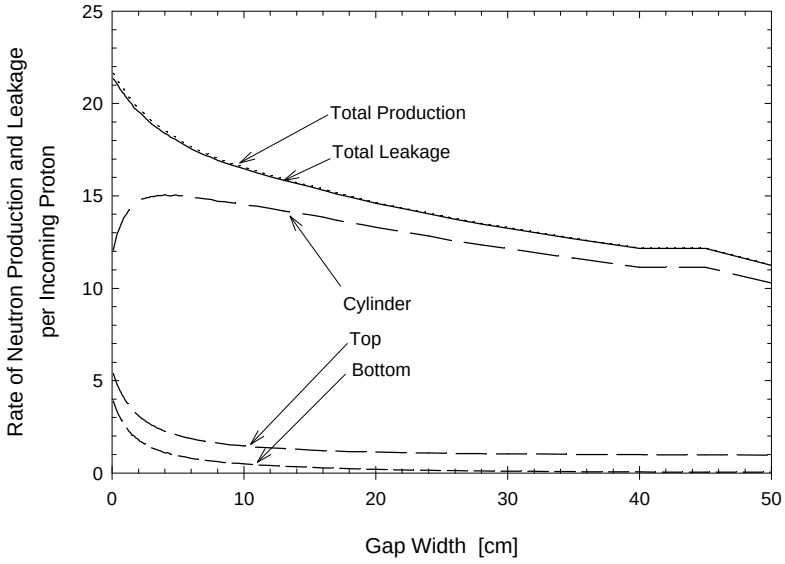
Rate of Neutron Production and Leakage
per Incoming Proton
25
20
15
10
5
0
0
10
20
30
40
50
Gap Width [cm]
Total Production
Total Leakage
Cylinder
Top
Bottom

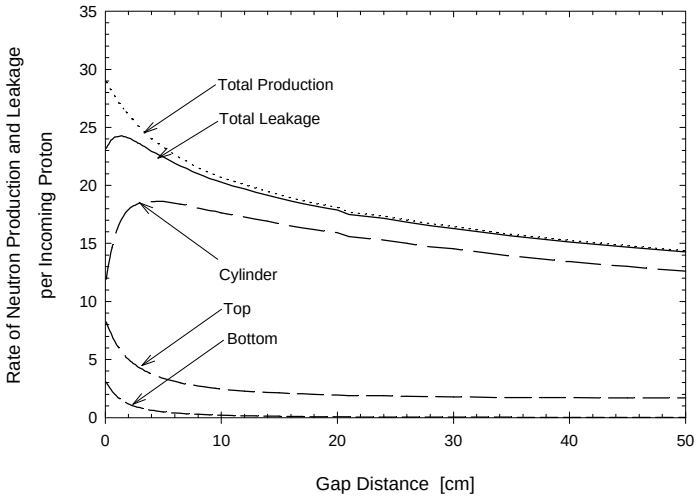
Rate of Neutron Production and Leakage per Incoming Proton
Gap Distance [cm]
Total Production
Total Leakage
Cylinder
Top
Bottom
0
5
10
15
20
25
30
35
0
10
20
30
40
50

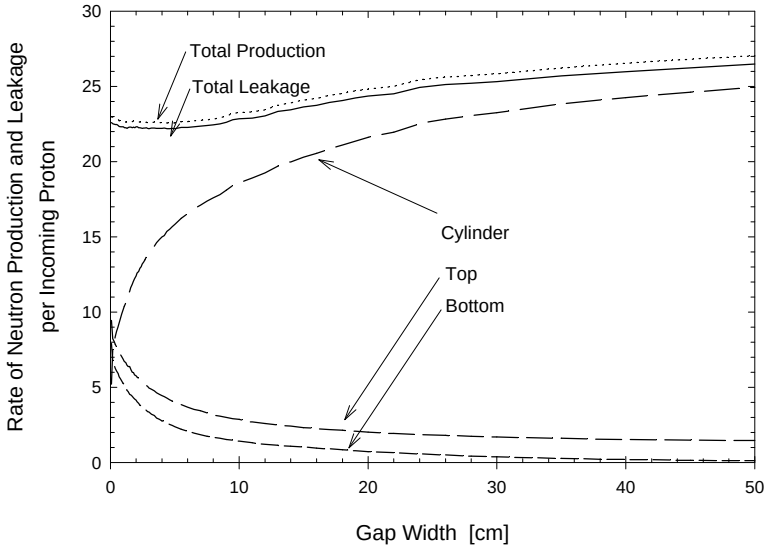
Rate of Neutron Production and Leakage
per Incoming Proton
Gap Width [cm]
Total Production
Total Leakage
Cylinder
Top
Bottom
0
5
10
15
20
25
30
0
10
20
30
40
50

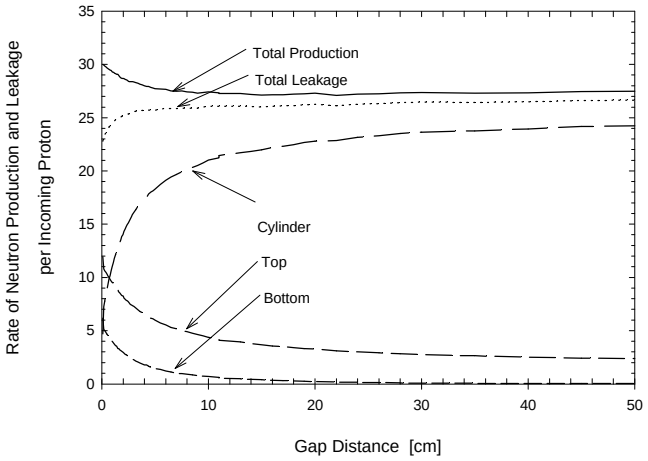
Rate of Neutron Production and Leakage
per Incoming Proton
Gap Distance [cm]
Total Production
Total Leakage
Cylinder
Top
Bottom
0
5
10
15
20
25
30
35
0
10
20
30
40
50

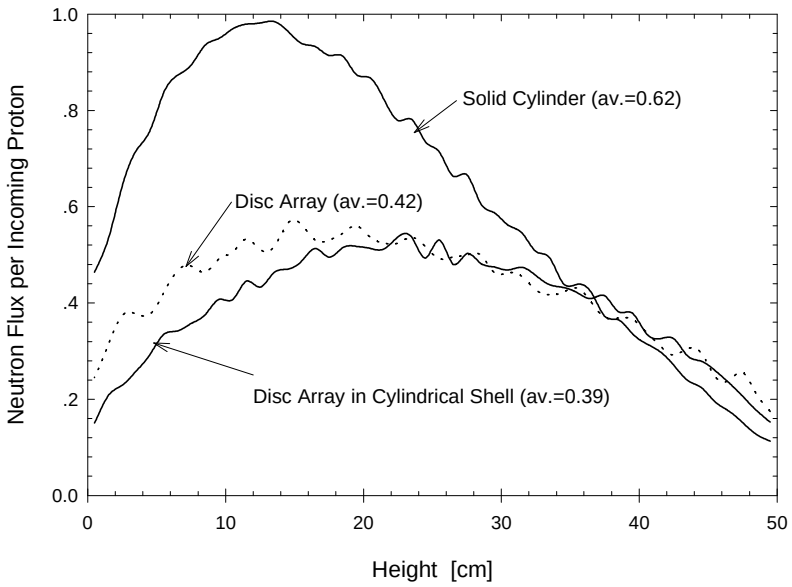
Neutron Flux per Incoming Proton
1.0
.8
.6
.4
.2
0.0
0
10
20
30
40
50
Height [cm]
Solid Cylinder (av.=0.62)
Disc Array (av.=0.42)
Disc Array in Cylindrical Shell (av.=0.39)

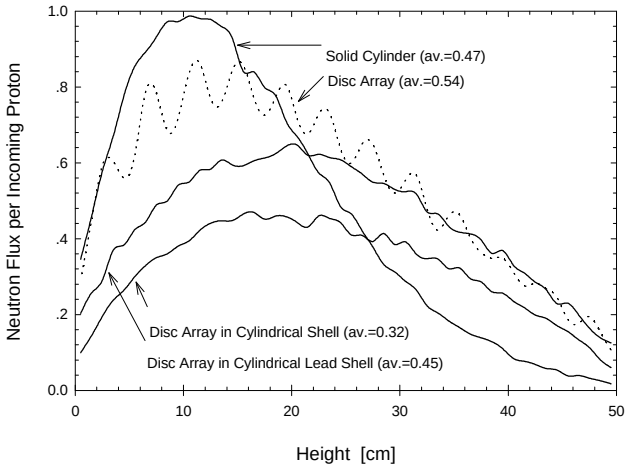
Neutron Flux per Incoming Proton
1.0
.8
.6
.4
.2
0.0
0
10
20
30
40
50
Height [cm]
Solid Cylinder (av.=0.47)
Disc Array (av.=0.54)
Disc Array in Cylindrical Shell (av.=0.32)
Disc Array in Cylindrical Lead Shell (av.=0.45)